Nanotechnology **21** (2010) 295303 (8pp) doi:10.1088/0957-4484/21/29/295303

Direct e-beam writing of dense and high aspect ratio nanostructures in thick layers of PMMA for electroplating

Sergey Gorelick, Vitaliy A Guzenko, Joan Vila-Comamala and Christian David

Paul Scherrer Institut, CH-5232 Villigen PSI, Switzerland

E-mail: sergey.gorelick@psi.ch

Received 17 February 2010, in final form 18 May 2010
Published 5 July 2010
Online at stacks.iop.org/Nano/21/295303

Abstract
Due to the ability of 100 keV electrons to penetrate deep into resist with little scattering, we were able to directly write various dense and high aspect ratio nanostructures in 540 nm and 1.1 μm thick layers of poly(methyl methacrylate) (PMMA) resist. The PMMA molds produced by electron beam lithography were developed using a high contrast developer. The molds were used to transfer the pattern into metallic nanostructures by filling the developed trenches with Au by electroplating. By exposing lines narrower than the target width, we observed improved process latitude and line width control. The obtained aspect ratios of the dense structures are nearly 20 in 1.1 μm PMMA layers and >16 for structures electroplated into this PMMA mold. The fabrication method was successfully applied to produce Au diffractive x-ray Fresnel zone plates of exceptionally good quality with 50 and 70 nm outermost zones using 540 nm and 1.1 μm thick PMMA molds. In addition, we also produced regular arrays of high aspect ratio and dense Au nanorods with periods down to 100 nm and high aspect ratio split-ring resonators.

(Some figures in this article are in colour only in the electronic version)

1. Introduction

Three dimensional, dense and high aspect ratio nanoscale structuring of noble metals is important for numerous optical applications. These include photonic crystals, plasmonic devices, metamaterials, x-ray lithography masks and diffractive x-ray optics.

In diffractive x-ray optics high aspect ratio Au structures are essential for high resolution and high efficiency devices, such as focusing Fresnel zone plates (FZP) [1]. The FZP is a chirped circular grating which period decreases with the radius (figure 1(a)). The width of the outermost ring (zone), Δr, in the FZP limits the size of the focused beam spot (both being comparable) and therefore the resolution of the x-ray nanoprobe. This means that if a sub-100 nm resolution is required, nanolithography processes with sub-100 nm resolution need to be applied when fabricating a FZP. Another important parameter is the diffraction efficiency of the FZP, i.e. fraction of the incident radiation that it is capable to concentrate in a focal spot[1]. This is determined by the height of the structures, t, the material they are made of, the photon energy and the line width accuracy. Even for high-Z materials, such as Au, the required height of the structures needs to be a micron or more for hard x-rays (6–12 keV photon energy) to provide acceptable efficiency. This means that the aspect ratio of the structures, $t/\Delta r$, must be more than ten when both high efficiency and resolution are required. In this paper we describe a fabrication method that utilizes 100 keV electron beam lithography in thick layers of PMMA that were used as electroplating molds to produce dense and high aspect ratio Au structures by electroplating.

This fabrication method can be useful not only in diffractive x-ray optics but also for production of other types of tall structures, and makes it possible to explore the behavior of 3D structures and compare it with the behavior of

[1] Since the diffraction efficiency decreases proportionally to m^{-2}, where m is the diffraction order, typically the first diffraction order is used as it is the most efficient.

 © 2010 IOP Publishing Ltd Printed in the UK & the USA

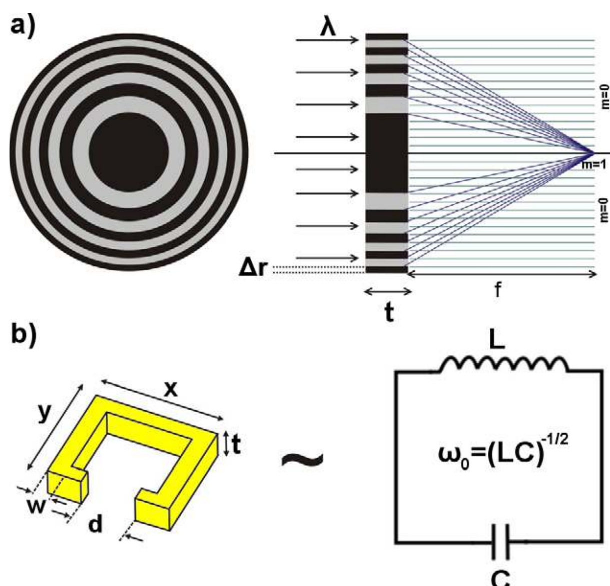

Figure 1. (a) Schematic presentation of a Fresnel zone plate that focuses radiation with wavelength λ in the first diffraction oder ($m = 1$). Some of the radiation passes the device undiffracted ($m = 0$), while some is diffracted into other diffraction orders ($m = 3, 5, -1, -3, -5$, etc) or absorbed. The size of the focused beam at $m = 1$ is roughly equal to the outermost zone, Δr, while the diffraction efficiency (proportion of the focused intensity with respect to the incident intensity) is determined by the height, t, of the device. (b) The split-ring resonator is a metallic structure mimicking an LC-circuit consisting of a capacitor, C, and a magnetic coil with inductance L with a resonant frequency at $\omega_0 = (LC)^{-1/2}$.

corresponding shallow structures. For instance, shallow split-ring resonators (SRRs) made of Au (figure 1(b)) were shown to exhibit plasmonic resonances at up to 1.5 μm wavelength of light [2]. Such resonances can be utilized for sensing small quantities of biological and chemical substances by detecting changes in the dielectric environment [3, 4]. The sensitivity of devices based on SRRs can be improved by increasing their height (aspect ratio) of the SRR structures which would increase the high-field region in the SRR gap thus raising the volume of the dielectric probed [5]. Furthermore, the resonance frequency has a tendency to increase with increased thickness of SRR [6]. The resonant responses can be extended to visible light frequencies by using materials composed of tall and dense Au nanorods instead of SRRs [7], while materials composed of dense high aspect ratio Ag nanorods were reported to have a negative index of refraction [8]. These nanorods were prepared by electroplating into the nanopores of anodized alumina [9, 10], which results in pseudo-ordered arrays of the nanorods. Some applications, however, may require highly ordered and uniform arrays of nanorods or more complex structures other than nanorods.

Among a plethora of lithographic methods, those capable of sub-micrometer or even sub-100 nm patterning of complex 3D dense and metallic structures are typically based on the interaction of energetic photons or charged particles with resist materials followed by filling of the resist mold by metals, e.g. by electroplating. Some of these methods include x-ray lithography (XRL), in which energetic photons are used to expose patterns through a mask [11–14], and proton beam writing (PWB) in which a focused beam of high energy (MeV) protons is used to directly write into very thick layers of photoresists [15–18]. However, both XRL and PBW are limited by difficulties associated with mask fabrication (XRL) or with the availability of beam time and commercial instruments (both XRL and PBW).

Instruments based on low energy (keV) focused ion beam (FIB) sputtering or deposition are commercially available. The advantage of FIB compared to other methods is that it does not require a resist and can be used on a variety of materials. However, even for a pure physical sputtering the realization of desired high aspect ratio dense structures is not straightforward [20], e.g. due to the redeposition of sputtered material and sputtering by the scattered ions. In addition, the writing speeds are typically low.

Electron beam lithography (EBL), on the other hand, is much faster. The primary interaction between low energy electrons (<30 keV) used in widely spread e-beam writers and the resist material is the transfer of energy to material's electrons in electron–electron collisions. However, because of the equal masses of electrons, the scattering angles are large and hence the forward scattering that broadens the beam with resist depth is significant. As the scattered electrons deviate further from the incident point when penetrating deeper into the resist and deposit energy along their trajectories, the lateral broadening of the exposed patterns becomes more pronounced with the resist depth. The forward scattering, therefore, leads to the 'pear shaped' ionization volume around the point of entry of electrons into resists [19]. As a result, the structures exposed in thick resists tend to have sloped walls, which can overlap if the patterns are exposed in close proximity to each other. Sub-100 nm, high aspect ratio and dense lithography, therefore, can be realized only in thin resist layers, although high aspect ratio structures can be fabricated using additional steps, e.g. reactive ion etching (RIE) and electroplating [21–24]. By increasing the electron beam energy to 100 keV the forward scattering can be reduced and dense, higher aspect ratio structures can be realized in a direct e-beam writing [25, 26].

In this paper we explored the possibility of fabricating dense and high aspect ratio nanostructures using 100 keV electron beam lithography in thick layers of PMMA and a high contrast developer. The developed resist patterns were used as molds for electroplating to produce Au structures. We chose Au because it is an attractive material for numerous applications (e.g., diffraction x-ray optics and plasmonics), however, the high aspect ratio PMMA molds can be used to transfer the patterns into other materials, such as Ni, Cu, Pt and many others [27]. Although 100 keV EBL in PMMA resist has been used before for fabrication of devices composed of high aspect ratio Au nanostructures (e.g. FZPs [28–30]), the process parameters and the ultimate resolution were not explored in detail. We optimized the process parameters (exposure, development time, and shrinkage of the design line width) such that the gratings with equal lines and spaces (duty cycle 0.5) were achieved with periods down to 80 nm and 110 nm for 540 nm and 1.1 μm thick PMMA layers, respectively. By exposing lines that were shrunk by a certain

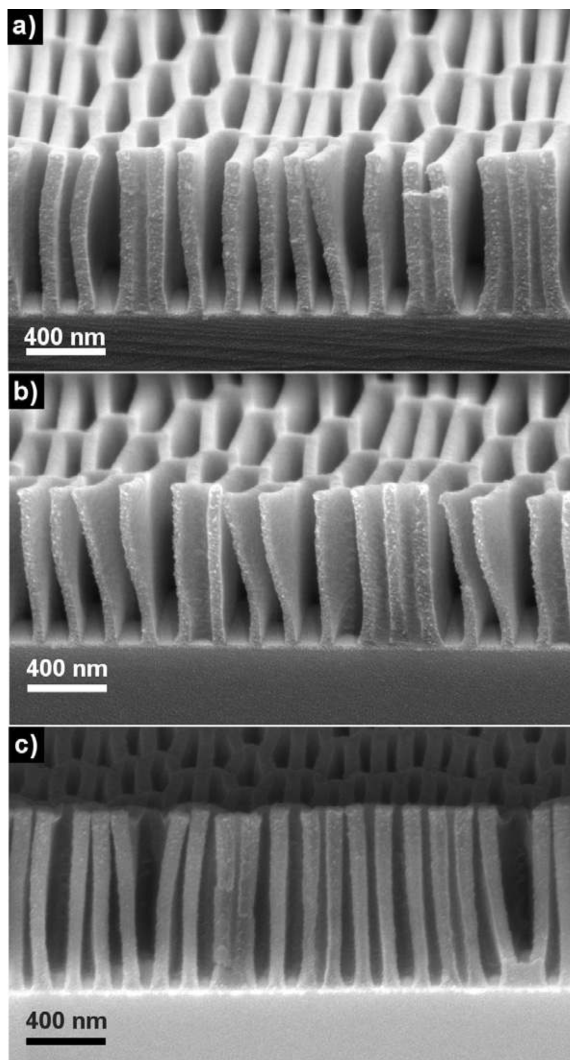

Figure 2. Scanning electron microscope (SEM) images of dense lines with support structures exposed in 1.1 μm thick PMMA on Cr/Si substrate (tilt 70°). The structures were coated with a few nm of Au prior to the SEM imaging. (a) Period 200 nm, shrinkage 40 nm (see text), 30 s development time. (b) Period 200 nm, shrinkage 40 nm, 60 s development time. (c) Period 160 nm, shrinkage 40 nm, 20 s development time. The PMMA lines were deformed during the cleaving of the samples and additionally deformed and shrank during the image acquisition with the SEM.

amount with respect to the target/design line widths, we were able to achieve significantly increased process latitude and vertical side walls, in addition to the improved minimum line width.

2. Experimental procedures

The fabrication process started by vapor-coating Si_3N_4 membranes[2] or bulk Si chips by Cr/Au plating base (5/20 nm) followed by evaporation of a 5 nm Cr layer on top of the Au layer. This upper Cr layer was proven to be necessary to promote a better adhesion of PMMA nanostructures,

[2] Fresnel zone plates are fabricated on thin silicon-nitride supporting membranes rather than on bulk substrates to reduce absorption of x-rays.

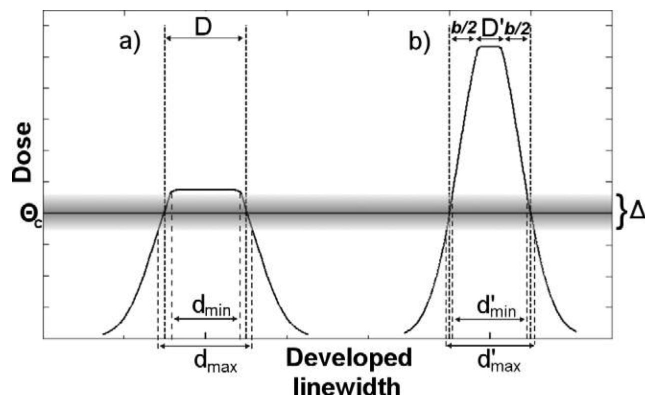

Figure 3. Schematic illustration of cross sectional dose profile in exposed lines in resist. The dose profiles are convolutions of the exposed rectangular shapes with the forward scattering of the electron beam in the resist and the Gaussian shape of the focused beam spot. The clearing dose is denoted by Θ_c, while the process latitude window is denoted by Δ. (a) Exposure of line width, D, equal to the target width. (b) Exposure of 'shrunk' line width, $D' = D - b$, with respect to the target width at increased dose. Due to the finite window of the process latitude, Δ, the developed line width variation for the shrunk line is smaller than for the unshrunk line.

which otherwise adhered weakly to the Au surface and delaminated from the substrate during the development or in the electroplating bath. Resist layers were spin-coated on Cr/Au/Cr/Si(or Si_3N_4) from a resist solution (4% of 950k PMMA in ethyl-lactate) at 1350 rpm for 120 s followed by a soft-bake at 180 °C for 5 min. This procedure yielded a ~540–550 nm thick resist layer, as measured with a profiler (DEKTAK 8, Veeco Instruments GmbH). To obtain a ~1.1 μm thick resist layer, the procedure was repeated twice.

The exposure of patterns was performed on a 100 keV electron beam writer (Vistec EBPG 5000plus) at 0.5–2 nA beam current. To find the optimal exposure parameters, we wrote a dose series of linear gratings that were designed to have equal lines and spaces, of various periods (40–600 nm), and with different line shrinkage, b, applied (between 0 and 50 nm). The half-shrinkage value, $b/2$, is termed 'bias' in the LayoutBeamer software (GenISys GmbH) that transforms the CAD files containing pattern information into the data format understood by the e-beam writer. The bias, $b/2$, applied to the lines in the patterns indicates the amount of line width shrinkage from each side of the lines, such that for a line that has a width d it means that a $(d-b)$-wide line will be exposed.

The development was performed by immersion of exposed chips in a mixture of isopropanol and water (7:3 by volume) followed by rinsing in de-ionized water and blow drying in a N_2 gas jet. This developer was chosen because it was reported to have good sensitivity, process latitude, and high contrast [32, 33]. Moreover, its viscosity is lower than that of conventional PMMA developers which allows efficient development of deep structures [18]. The development time was optimized to 10 s and 20 s for 540 nm and 1.1 μm thick PMMA layers, respectively.

Initial tests showed that long PMMA lines collapsed after the development step presumably due to the action

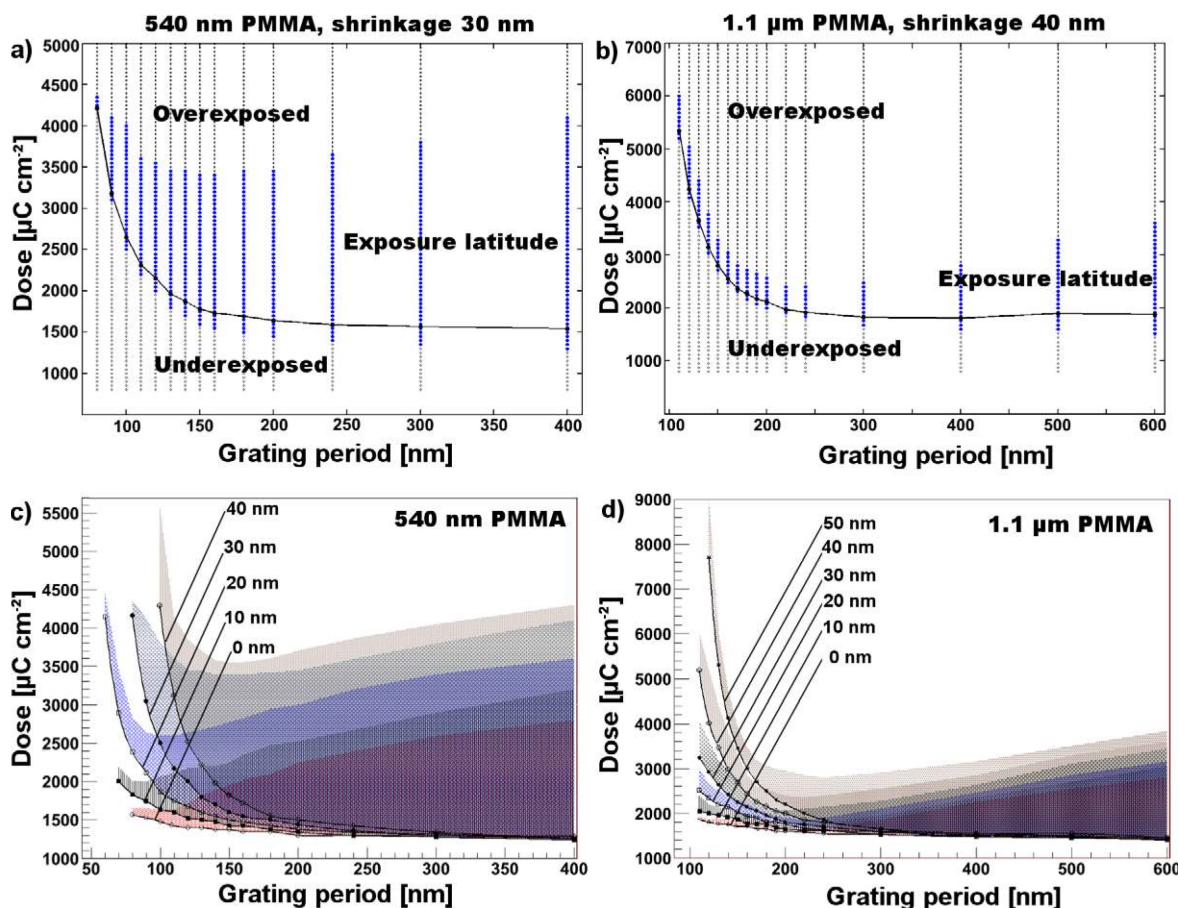

Figure 4. Area doses and exposure latitude for gratings of different periods exposed in PMMA for 30 nm and 40 nm line shrinkages in (a) 540 nm thick PMMA and (b) 1.1 μm thick PMMA, respectively. The black lines show the doses (typically 10–20% above the critical doses) that were used in exposures of Fresnel zone plates (figure 7). ((c), (d)) Area doses and exposure latitude for gratings of different periods exposed in 540 nm thick PMMA and 1.1 μm thick PMMA and for various shrinkages (0–50 nm).

of the capillary forces during drying. To improve the polymer mold stability the long lines were divided into segments that were exposed while leaving short unexposed separations between the segments. After the development, the PMMA structures resembled lines interconnected by supporting 'bridges' (figure 2). The mechanical stability of such interconnected PMMA lines depends on their width and height, the length of the 'bridges' that interconnect the lines, the length of the segments, and the structural organization of the 'bridges' [23, 31]. No systematic study was performed to optimize these parameters in order to maximize the segment length, but in general for 50–80 nm wide 'bridges' and segments 5–12 times longer than their width, the resulting interconnected PMMA mold was rigid after the development.

After the development, the samples were treated by Cl_2/CO_2 plasma to remove the upper Cr layer. This was necessary to reveal the underlying Au layer before the electroplating. This plasma treatment does not affect the PMMA mold significantly. The developed trenches in PMMA were then filled with Au by electroplating in a cyanide-based plating bath at a plating current density of 2.5 mA cm^{-2}. The PMMA mold was later removed by ashing in O_2 plasma.

The electroplating results in 'dashed line' structures instead of continuous lines. Such interrupted lines result in somewhat reduced efficiency of devices in diffractive x-ray optics applications. However, much greater losses of the diffraction efficiency are associated with mechanical instability of the structures due to the collapse of continuous lines. It is, therefore, better to sacrifice the line integrity thus preventing the pattern collapse. In principle, the pattern collapse can be reduced by using supercritical drying in CO_2, however, to the best of our knowledge, no process compatible with the PMMA resist exists. We attempted to optimize the supercritical process for dense PMMA structures, however, the drying process typically ended in a complete destruction of the test gratings.

3. Results and discussion

Our goal was to optimize the process parameters such that the 0.5 duty cycle (line-width-to-period ratio) of gratings was ensured. The exposure of the lines 'designed-as-desired' typically results in the line broadening. The line broadening is attributed to the Gaussian beam spot profile and forward scattering of the electrons. The dose profile in the resist is, therefore, a convolution of the exposed pattern, the beam spot, the range of secondary electrons and the forward scattering (figure 3). Due to the finite process

latitude window, Δ, stemming from the variations in the process parameters (e.g. variations in the development time, temperature, developer concentration, etc), the exposure of the patterns as-designed can result in significantly wider or narrower structures than intended, because the convoluted dose profile can vary greatly within the process latitude around the clearing dose Θ_c (figure 3(a)). On the other hand, the exposure of shrunk patterns with respect to the target size at increased doses enables us to adjust the process parameters such that the clearing dose is reached at the desired pattern dimensions. In this case, the dose profile variations at the clearing dose and within the process latitude window, Δ, are small, such that the line width variations are also reduced (figure 3(b)). Exposing shrunk lines also enables us to greatly improve the exposure latitude, such that the dimensions of the exposed patterns are affected to a lesser degree when the exposure dose or development parameters deviate from the optimum.

To optimize the development time, we exposed a dose series of linear gratings in PMMA applying different shrinkages and that were developed for different times. Figure 2 shows PMMA gratings that were produced using a shrinkage of 40 nm and different development times. Since we needed to optimize at least three parameters simultaneously (development time, shrinkage and exposure dose), we chose first to optimize the development time, then exposure doses and finally the shrinkage.

During the development step, the dissolution front is advancing vertically into the PMMA (vertical development). Simultaneously, an additional dissolution front is advancing laterally (side-wall development). Hence, longer development time typically causes line width broadening (compare figure 2(a), 30 s development and figure 2(b), 60 s development), shorter development will result in decreased line width broadening (but requires higher exposure dose). The line broadening has a low limit for particular line shrinkage and development time; because of that, the line broadening cannot be efficiently controlled by reducing the dose, since the reduced dose may result in an incompletely developed line that does not reach the substrate. The side-wall development is considerably slower than the vertical development due to the larger molecular weight of the PMMA fragments found at the features edges that receive reduced exposure doses. Decreasing the development time can, therefore, reduce the line broadening. It is of benefit to keep the line broadening and thus the necessary shrinkage, b (needed to offset the broadening), to the minimum, because otherwise no line width smaller than b can be exposed. By reducing the development time from 30 to 20 s, we were able to obtain a 160 nm period grating with a 0.5 duty cycle (figure 2(c)) using the same line shrinkage of 40 nm as in the case of 30 s development where 0.4 duty cycle and 200 nm period grating was obtained (figure 2(a)). In the latter case, the shrinkage of 50 nm would be required to keep the desired line width to a period ratio of 0.5, hence, no line width <50 nm is possible. We chose to keep the 20 s and 10 s development times for 1.1 μm PMMA and 540 nm PMMA layers, respectively. Reducing these development times is of no further advantage, because the required exposure dose increases which consequently causes more line width broadening than is gained by decreasing the development time.

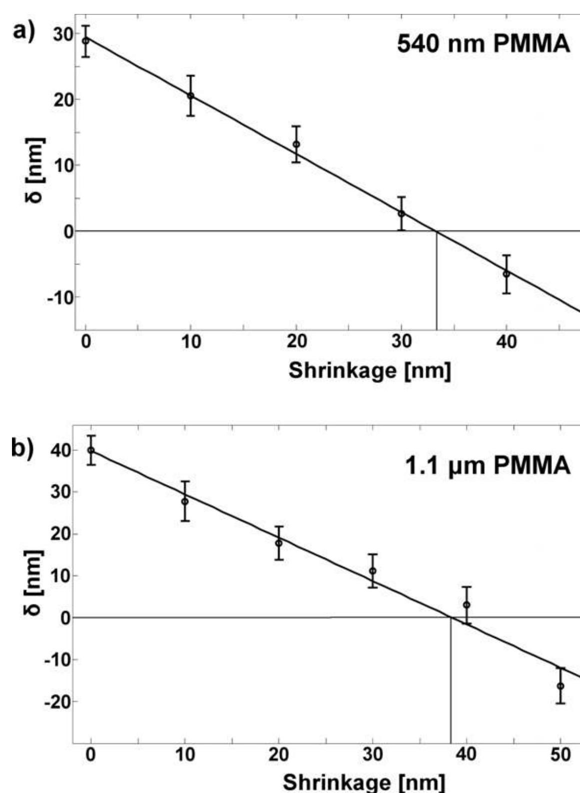

Figure 5. Line width broadening in gratings, δ, at the clearing dose as a function of the line shrinkage for 540 nm and 1.1 μm thick PMMA layers and for 10 s and 20 s development time, respectively, in a mixture of isopropanol and water (7:3 by volume). The broadening is defined as $\delta = d_{\text{meas}} - P/2$, where d_{meas} is the measured line width and P is the grating period. The shrinkages of $\sim$33 nm and $\sim$38 nm result in the optimal grating duty cycle of 0.5 in 540 nm and 1.1 μm thick PMMA, respectively.

After we chose the development times, we exposed a dose series of 20 μm × 20 μm gratings in PMMA and applied a wide range of shrinkages in order to find the optimal shrinkage-dose parameters that result in gratings with a 0.5 duty cycle. These PMMA gratings were used as molds for electroplating, which was also a way to see whether the structures were fully developed. If the structures were underexposed, a thin resist layer remained on the substrate and consequently the electroplating could not start. The times required to fully develop the high aspect ratio nanostructures can be substantially longer than that for wide structures, because of constrained diffusion of PMMA fragments from the confined PMMA nanochannels. The development time for narrow lines can be reduced by exposing them with higher doses, which decreases the molecular weight of PMMA fragments and promotes their diffusion. Therefore, if the resist is patterned with both large and small features, the exposure dose should be adjusted according to the features' sizes. Figure 4 presents measured clearing doses and the exposure latitude for gratings of different periods and line shrinkage. The upper limit of the exposure latitude was defined as the dose at which the line width is increased by 20% or when the structural integrity of

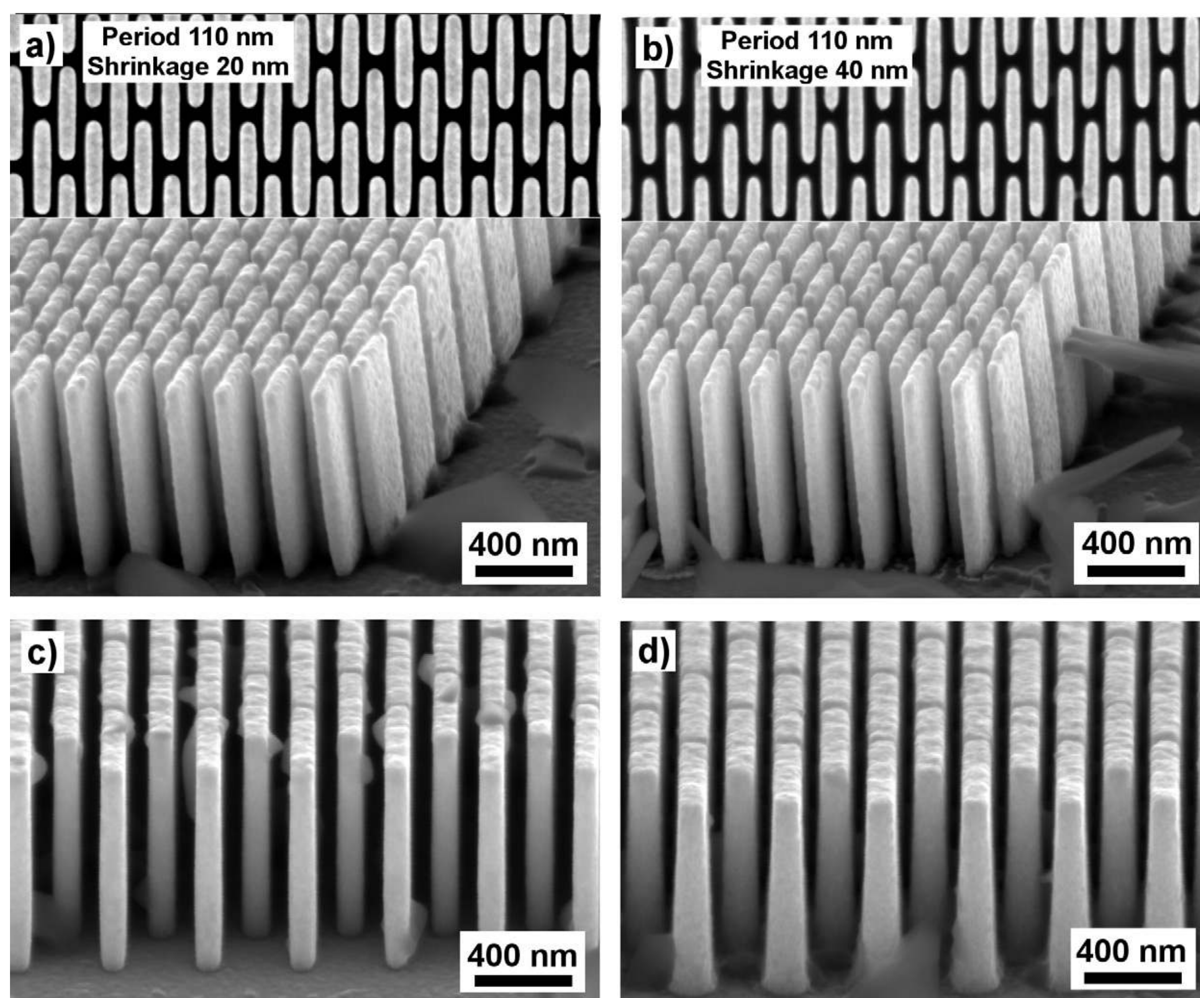

Figure 6. Scanning electron microscope images of 'dashed line' gratings produced by electroplating 900 nm of Au into 1.1 μm PMMA molds that were directly exposed by 100 keV electrons at various line shrinkages. Period 110 nm lines for (a) shrinkage 20 nm, (b) shrinkage 40 nm. Period 200 nm lines exposed with a 30 nm shrinkage (c) dose close to the clearing dose, (d) significantly overexposed.

the pattern is lost (e.g. due to overexposure). The definition of exposure latitude varies in literature, but can be typically defined as a range of doses within which the pattern dimension varies to the extent of $\pm 10\%$ [34]. In this study, however, the pattern line width has a minimal size (at the clearing dose) below which it cannot decrease, since for a lower dose the line would be underexposed. For a grating having the optimal duty cycle allowing the line width to increase by 20% means that the duty cycle can increase to 0.6, which for diffractive x-ray optics applications leads to only a minor decrease in the device's diffraction efficiency.

In addition to being a method to improve the process latitude, the line shrinkage is also a way to control the line width in gratings. We noticed that the broadening from the optimal line width in a linear grating depends mainly on the shrinkage and is nearly independent of the grating period. From figure 5 which presents the measured line broadening versus the shrinkage at the clearing dose, the optimal shrinkage is 33 ± 2.1 nm and 38 ± 2.4 nm for 540 nm and 1.1 μm thick PMMA layers, respectively. Figures 6(a) and (b) compare high aspect ratio Au gratings (110 nm period) that were exposed using 20 nm and 40 nm shrinkage, respectively. The duty cycle in the latter case is optimal and equal to nearly 0.5, whereas in the grating where the 20 nm shrinkage was used, the duty cycle of $\sim$0.7 is not optimal. The height of the gratings in figure 6 is 900 nm, meaning that Au was not electroplated up to the resist top. Hence, the aspect ratio of lines in figure 6(b) is greater than 16, which means that the aspect ratio of the initial 1.1 μm high PMMA mold was almost 20. To our knowledge, this is the highest aspect ratio achieved so far with electron beam lithography in PMMA for dense nanostructures. The shrinkages (33–38 nm) that we found for the presented process conditions (development time and developer) represent the lowest line width obtainable with this method in the two PMMA thicknesses in a single pixel exposure. This means that the highest aspect ratio for dense patterns can be up to 15–16 in 550 nm PMMA and even up to 27–28 in 1.1 μm PMMA. However, the process/exposure latitude window for a single pixel exposure is extremely narrow (figure 4) and obtaining such high aspect ratio structures is challenging. The line broadening and hence the required shrinkage needed to offset this broadening can potentially be decreased by further optimizing the process parameters [35]. Thus, using cold development was shown to

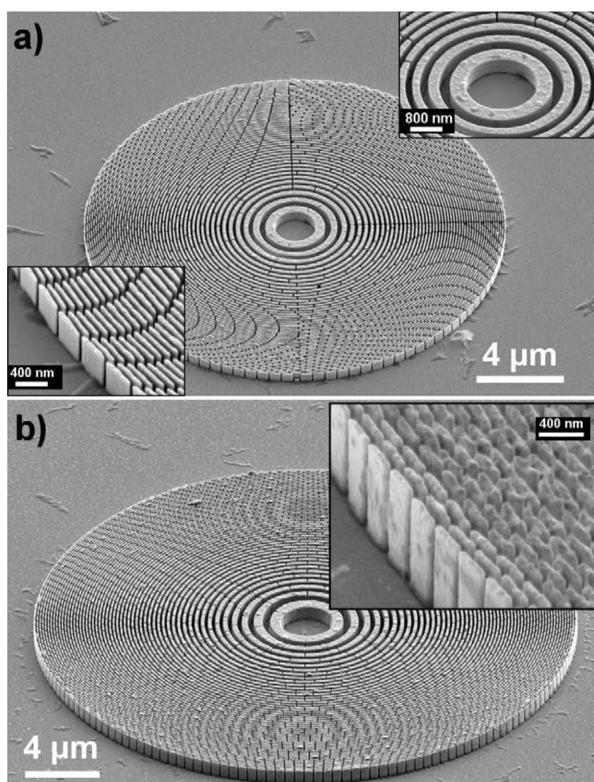

Figure 7. Scanning electron microscope image of (a) 0.5 μm and (b) 1 μm thick Fresnel zone plates fabricated by electroplating Au in PMMA molds that were produced by directly writing into the resist with 100 keV electrons. The insets present magnified inner and outer regions of the devices.

enhance the resolution in PMMA compared to conventional room temperature development [36] because the developer mainly removed central regions of the exposed lines where lower molecular weight of PMMA fragments was produced by the higher electron beam dose. Using cold development can, therefore, help to slow down the dissolution front from advancing laterally (side-wall development) where heavier PMMA fragments are located, and consequently reduce the lateral broadening and hence the required shrinkage. The use of ultrasonic [33, 37] or megasonic [38] development was also shown to aid the development of high aspect ratio nanostructures, to increase the resolution, thus being beneficial for reduction of the required shrinkage. We therefore believe that the presented aspect ratios for dense structures can be further improved by applying cold development assisted by ultrasonic or megasonic agitation.

In order to fabricate functional devices we typically used doses which are 10–15% above the clearing doses (figure 4), which was necessary to compensate for the uncertainties in development times and developer temperature. The optimal shrinkages in such a case are 35 nm and 40 nm for 540 nm and 1.1 μm PMMA layers, respectively. As we mentioned above, the width of lines can increase up to 20% with increased dose within the exposure latitude window (figure 4). In addition to the line width broadening, the shape of the lines is also altered with the increase in exposure dose. Figures 6(c) and (d) compare the lines obtained at the clearing dose and

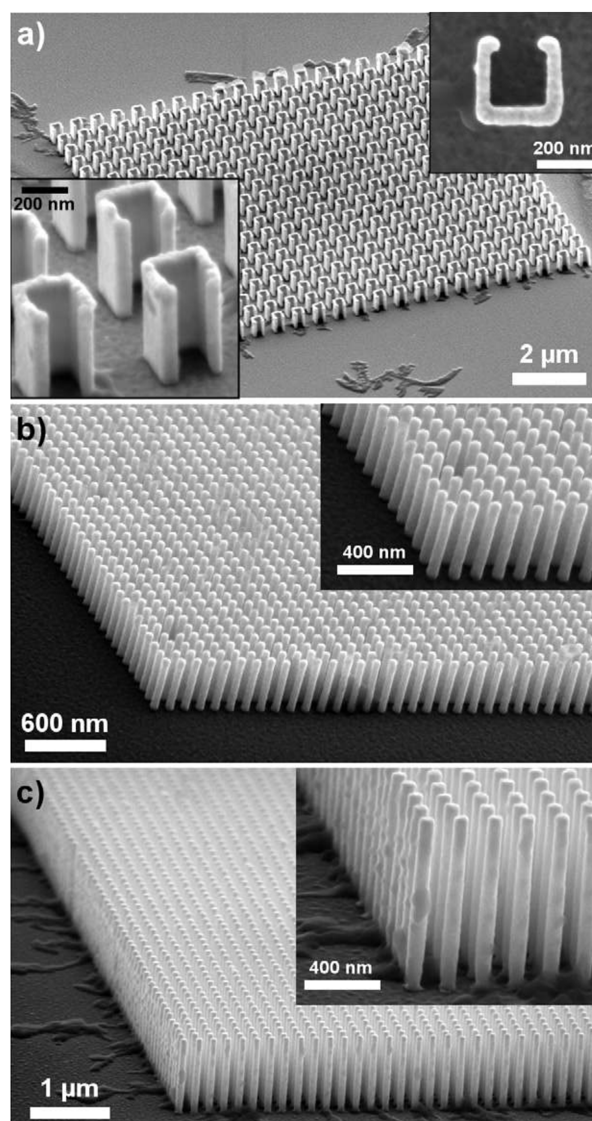

Figure 8. High aspect ratio structures fabricated by electroplating into molds exposed in thick layers of PMMA. (a) 450 nm tall split-ring resonators with a line width of 40–45 nm. Nanorods (b) period 100 nm and height 450 nm, (c) period 180 nm and height 950 nm.

that were severely overexposed, respectively. The lines that were exposed with low dose have vertical side walls, whereas overexposed lines are significantly broadened and have sloped walls. Thus, using the exposure dose to control the line width is not optimal, since higher doses result in sloped rather than vertical side walls.

Figure 7 shows complex patterns (Fresnel zone plates) composed of dense features with sizes ranging from several tens and up to several hundreds of nm, that were exposed using the dose modulation from figure 4 for 30 nm shrinkage in 540 nm PMMA (figure 7(a)) and 40 nm shrinkage in 1.1 μm PMMA (figure 7(b)). The zone plates are uniform and are of exceptionally good quality. Since we either used thin membranes as substrates or wrote small areas with large separations between them, the proximity effect is negligible. For large patterns on bulk substrates proximity correction

needs to be done to ensure the correct dose across the whole pattern.

In addition to high aspect ratio Fresnel zone plates and gratings, the method can be applied to produce a variety of structures. Figure 8 shows dense arrays of split-ring resonators (figure 8(a)) and nanorods (figures 8(b) and (c)) that can potentially be used in plasmonic and biosensing devices. Although the exposure doses need to be optimized for a particular pattern, the optimization is straightforward, and similar shrinkage values as for the linear gratings (~40 nm) can be applied to yield the desired pattern dimensions. It should be kept in mind that if a structure is made up of lines of various widths, the dose should be optimized for different parts of the structure such that a simultaneous development of all of the line widths is assured.

4. Conclusion

We have optimized exposure and development parameters of high aspect ratio dense nanostructures in thick layers (up to 1.1 μm) of PMMA resist. Using 100 keV electrons and high contrast developer we produced 0.5-duty-cycle 110 nm period linear gratings of 'dashed line' configuration in 1.1 μm thick PMMA and transferred the pattern into 900 nm tall Au gratings by electroplating. This corresponds to an aspect ratio of 16 in Au and almost 20 in the resist. Although the achievable aspect ratios in 1 μm PMMA are higher than those in 0.5 μm PMMA, the resolution in the latter case is higher with lines down to 40 nm. Using optimized line shrinkage and dose as a function of the grating period, we fabricated high quality Au Fresnel zone plates with 50 nm and 70 nm outermost zones in 540 nm and 1.1 μm thick PMMA, respectively. In addition to the Fresnel zone plates, we fabricated high aspect ratio split-ring resonators and arrays of nanorods with periods down to 100 nm, that can have a potential use in plasmonic and biosensing devices.

Acknowledgments

We would like to thank Martin Bednarzik, Bianca Haas, Anja Weber, Eugen Deckhardt and Arnold Lücke for assistance during substrate preparation. This work has been carried out under the auspices of Collaborative Project NFFA—Nanoscale Foundries and Fine Analysis, contract No. 212348, of the Seventh EU Framework Programme. The research leading to these results has also received funding from the European Community's Seventh Framework Programme (FP7/2007-2013) under grant agreement 226716.

References

[1] see, for example: Howells M, Jacobsen C, Warwick T and van den Bos A 2008 *Principles and Applications of Zone Plate X-Ray Microscopes* (*Science of Microscopy*) ed P W Hawkes and J C H Spence (New York: Springer) pp 835–926, ISBN 978-0-387-25296-4 (Print) 978-0-387-49762-4 (Online) 2008
[2] Enkrich C, Wegener M, Linden S, Burger S, Zschiedrich L, Schmidt F, Zhou J F, Koschny Th and Soukoulis C M 2005 *Phys. Rev. Lett.* **95** 203901
[3] Debus S and Bolivar P H 2007 *Appl. Phys. Lett.* **91** 184102
[4] Al-Naib I A I, Jansen C and Koch M 2008 *Appl. Phys. Lett.* **93** 083507
[5] Chiam S-I, Singh R, Gu J, Han J, Zhang W and Bettiol A A 2009 *Appl. Phys. Lett.* **94** 064102
[6] Guo H, Liu N, Fu L, Schweizer H, Kaiser S and Giessen H 2007 *Phys. Status Solidi* b **244** 1256
[7] Kabashin A V, Evans P, Paskovsky S, Hendren W, Wurtz G A, Atkinson R, Pollard R, Podolskiy V A and Zayats A V 2009 *Nat. Mater.* **8** 867
[8] Yao J, Liu Z, Liu Y, Wang Y, Sun C, Bartal G, Stacy A M and Znang X 2008 *Science* **321** 930
[9] Masuda H and Fukuda K 1995 *Science* **268** 1466
[10] Yin A J, Li J, Jian W, Bennet A J and Xu J M 2001 *Appl. Phys. Lett.* **79** 1039
[11] Flanders D C 1980 *Appl. Phys. Lett.* **36** 93
[12] Chu W, Smith H I and Schattenburg M L 1991 *Appl. Phys. Lett.* **59** 1641
[13] Lai B *et al* 1992 *Appl. Phys. Lett.* **61** 1877
[14] Krasnoperova A A *et al* 1993 *J. Vac. Sci. Technol.* B **11** 2588
[15] Watt F, Breese M B H, Bettiol A A and van Kan J A 2007 *Mater. Today* **10** 20
[16] van Kan J A, Bettiol A A and Watt F 2003 *Appl. Phys. Lett.* **83** 1629
[17] van Kan J A, Bettiol A A and Watt F 2006 *Nano Lett.* **6** 579
[18] Ansari K, van Kan J A, Bettiol A A and Watt F 2004 *Appl. Phys. Lett.* **85** 476
[19] Drouin D, Couture A R, Joly D, Tastet X, Aimez V and Gauvin R 2007 *Scanning* **29** 92–101
[20] Platzgummer E *et al* 2006 *Microelectron. Eng.* **83** 936
[21] Schneider G, Schliebe T and Aschoff H 1995 *J. Vac. Sci. Technol.* B **13** 2809
[22] Jefimovs K, Bunk O, Pfeiffer F, Grolimund D, van der Veen J F and David C 2007 *Microelectron. Eng.* **84** 1467
[23] Feng Y, Feser M, Lyon A, Rishton S, Zeng X, Chen S, Sassolini S and Yun W 2007 *J. Vac. Sci. Technol.* B **25** 2004
[24] Lindblom M, Hertz H M and Holmberg A 2007 *Microelectron. Eng.* **84** 1136
[25] Rooks M J, Kratschmer E and Viswanathan R 2002 *J. Vac. Sci. Technol.* B **20** 2937
[26] Lu M, Ocola L E, Divan R and Mancini D C 2008 *Proc. SPIE* **7039** 70390V
[27] Lowenheim F 1978 *Electroplating* (New York: McGraw-Hill) ISBN 0070388369
[28] Chen Y T *et al* 2008 *Nanotechnology* **19** 395302
[29] Chen Y T *et al* 2008 *J. Synchrotron Radiat.* **15** 170
[30] Lo T N *et al* 2007 *J. Phys. D: Appl. Phys.* **40** 3172
[31] Gorelick S, Vila-Comamala J, Guzenko V, Mokso R, Stampanoni M and David C 2009 *Microelectron. Eng.* **87** 1052
[32] Yasin S, Hasko D G and Ahmed H 2002 *Microelectron. Eng.* **61/62** 745
[33] Yasin S, Hasko D G and Ahmed H 2001 *Appl. Phys. Lett.* **78** 2760
[34] Cui Z 2005 *Micro-Nanofabrication. Technologies and Applications* (Beijing: Higher Education Press) ISBN 7-04-017663-7
[35] Grigorescu A E and Hagen C W 2009 *Nanotechnology* **20** 292001
[36] Hu W, Sarveswaran K, Lieberman M and Bernstein G H 2004 *J. Vac. Sci. Technol.* B **22** 1711
[37] Chen W and Ahmed H 1993 *Appl. Phys. Lett.* **62** 1499
[38] Küpper D, Küpper D, Wahlbrink T, Bolten J, Lemme M C, Georgiev Y M and Kurz H 2006 *J. Vac. Sci. Technol.* B **24** 1827